

February 6, 2020

Thermodynamics of clusterized matter

Ad. R. Raduta¹ and F. Gulminelli²

¹ NIPNE, Bucharest-Magurele, POB-MG6, Romania,

² LPC (IN2P3-CNRS/Ensicaen et Université), F-14076 Caen cédex, France

Thermodynamics of clusterized matter is studied in the framework of statistical models with non-interacting cluster degrees of freedom. At variance with the analytical Fisher model, exact Metropolis simulation results indicate that the transition from homogeneous to clusterized matter lies along the $\rho = \rho_0$ axis at all temperatures and the limiting point of the phase diagram is not a critical point even if the surface energy vanishes at this point. Sensitivity of the inferred phase diagram to the employed statistical framework in the case of finite systems is discussed by considering the grand-canonical and constant-pressure canonical ensembles. A Wigner-Seitz formalism in which the fragment charge is neutralized by an uniform electron distribution allows to build the phase diagram of neutron star matter.

PACS numbers: 25.70.Mn, 64.70.F-, 26.60.-c 64.60.an,

I. INTRODUCTION

Droplet models constitute a suitable tool to study structural ordering transitions. Freezing, condensation and glassiness together with metallic alloys phase transitions illustrate both the phenomena diversity and the multitude of domains which benefit from them [1].

At sub-atomic scale, clusterized nuclear matter is expected to be present in the cores of exploding supernovae [2, 3, 4, 5] and in the inner crust of neutron stars [6, 7, 8, 9, 10, 11, 12, 13] where the interplay between surface and Coulomb energy is responsible for the occurrence of exotic pasta phases at densities close to the saturation density of nuclear matter.

Concerning finite nuclear systems, the presumptive existence of the so-called break-up stage in the simultaneous multi-particle decay of excited nuclei persuaded Finn *et al.* [14, 15] to address nuclear multifragmentation in terms of a (critical) evaporation according to Fisher cluster theory [16] as early as the '80s. Sophisticated analyzes of high quality data accumulated over more than two decades confirm this scenario [17, 18, 19, 20, 21, 22] and point-out that a first-order phase transition occurs as well [23, 24, 25, 26, 27, 28].

These data have been over the years well described by statistical models with cluster degrees of freedom [29, 30, 31, 32]. These studies confirm the occurrence of a liquid-gas phase transition in finite excited nuclei [33], irrespective of the presence of the non-saturating Coulomb interaction [34]. Much less ambiguous is their answer to the criticality issue, as fragment size scaling is obtained in a broad region of the phase diagram, probably due to the system finite size [35].

The aim of the present paper is to investigate the shape of the phase diagram of infinite neutral clusterized matter and under which conditions a critical behavior is obtained.

Sec. II discusses the thermal and phase properties of nuclear matter as obtained by an exact Metropolis Monte-Carlo model with respect to the predictions of the analytical Fisher model. Phase coexistence is inferred out of the bimodal behavior of state variable distributions. The phase diagram manifests first and second order phase transitions; the dense phase lies along the $\rho = \rho_0$ line, while phase coexistence characterized by clusterized partitions manifests over a broad density domain. Critical behavior in the vicinity of the limiting point is studied via the hyperscaling relations connecting critical exponents. Contrary to the predictions of the analytical Fisher model, it results that the vanishing fragment surface energy is not a sufficient condition to obtain a critical behavior at the limiting point, though fragment properties give rise to critical exponents β and γ in acceptable agreement with the values of the LG universality class.

Sec. III analyzes the sensitivity of small systems to the considered thermodynamical framework, while the phase diagram of neutron star matter in the Wigner-Seitz approximation is presented in Sec. IV. Conclusions are drawn in Sec. V.

II. THE CLUSTER MODEL

It is theoretically well settled that uniform nuclear matter is instable to density fluctuations of finite wavelength in a wide region of densities and temperatures, leading to spontaneous cluster formation [36, 37]. The same is true for stellar matter [38, 39, 40], and the physical properties at the crust-core transition point are of special interest for astrophysical purposes [41]. A description of the thermodynamical properties of these systems can be obtained introducing a statistical model with cluster degrees of freedom. Such an approach was proposed by Fisher in the late sixties to describe the process of condensation close to a critical point [16].

Under the equilibrium assumption, the statistical approach of a system broken into N pieces reduces the physical problem to the estimation of the number of microscopic states compatible with the thermodynamical macroscopic constraints. For instance, in the simple case of a 1-component fluid, if one ignores the internal excitation, position, momenta, spins and parities of the clusters, a configuration will be exclusively defined by fragment sizes,

$$k : \{A_1, \dots, A_{N_k}\}. \quad (1)$$

Including isotopic, translational and internal degrees of freedom, as it is usually done to treat the particular case of nuclear multifragmentation, leads to:

$$k : \{A_1, Z_1, e_1, \vec{r}_1, \vec{p}_1, \dots, A_{N_k}, Z_{N_k}, e_{N_k}, \vec{r}_{N_k}, \vec{p}_{N_k}\}, \quad (2)$$

where A_i , Z_i , e_i , \vec{r}_i and \vec{p}_i stand for the mass, charge, internal energy, center-of-mass position and momentum of each fragment.

Assuming that it is possible to write down a tractable expression for the statistical weight of the configuration W_k in the statistical ensemble suitable for the phenomenon under study, one can express the characteristic partition sum Z and any ensemble-averaged observable $\langle X \rangle$ as a function of the statistical weight of the configuration W_k ,

$$Z = \sum_{(k)} W_k, \quad (3)$$

and, respectively,

$$\langle X \rangle = \frac{\sum_{(k)} X^{(k)} W_k}{\sum_{(k)} W_k}. \quad (4)$$

Many improvements and sophistications can and have to be added to describe the nuclear multifragmentation problem [32] or the stellar equation of state [4, 8], but in this section we shall only focus on one-component clusterized systems in the grandcanonical ensemble. This will allow for a direct comparison between results obtained analytically at the thermodynamic limit and predictions of Monte-Carlo methods.

A. The analytical Fisher model

In the grand-canonical ensemble, the generic expression of the partition function of an infinite one-component system composed of independent clusters reads,

$$Z_{\beta, \beta\mu} = \sum_{(k)} \exp \left[-\beta \left(E_{tot}^{(k)} - \mu A_{tot}^{(k)} \right) \right], \quad (5)$$

with,

$$E_{tot}^{(k)} = \sum_{A=1}^{\infty} n_A^{(k)} e(A); \quad (6)$$

$$A_{tot}^{(k)} = \sum_{A=1}^{\infty} n_A^{(k)} A, \quad (7)$$

where $n_A^{(k)}$ is the multiplicity of fragments of size A in the (k) -class of events, $e(A)$ is the cluster energy functional, and for the moment we ignore the degeneracy of the different energy states for each fragment size. The interest of the Fisher cluster model [16] is that the partition sum can be expressed as a product of individual cluster partition sums,

$$\mathcal{Z}_{\beta,\beta\mu} = \prod_{A=1}^{\infty} z_{\beta,\beta\mu}(A), \quad (8)$$

where

$$\begin{aligned} z_{\beta,\beta\mu}(A) &= \sum_{n_A} \exp [-\beta n_A (e(A) - \mu A)] \\ &= 1 \pm \exp [-\beta (e(A) - \mu A)], \end{aligned} \quad (9)$$

and the $+$ ($-$) accounts for Fermi (Bose) statistics of the clusters states. If we consider the classical Boltzmann limit of a huge number of available states, $n_A \ll 1$ we get,

$$\omega_{\beta,\beta\mu}(A) = \ln z_{\beta,\beta\mu}(A) \approx \exp [-\beta (e(A) - \mu A)], \quad (10)$$

leading to,

$$\mathcal{Z}_{\beta,\beta\mu} = \prod_{A=1}^{\infty} \sum_{n_A=0}^{\infty} \frac{\omega_{\beta,\beta\mu}^{n_A}(A)}{n_A!}, \quad (11)$$

or, equivalently,

$$\ln \mathcal{Z}_{\beta,\beta\mu} = \sum_{A=1}^{\infty} \omega_{\beta,\beta\mu}(A), \quad (12)$$

with $\omega_{\beta,\beta\mu}(A)$ given by Eq. (10).

Taking now into account that the clusters may be excited and have translational degrees of freedom $e_n(A, \vec{p}) = e_n(A) + p^2/2Am$, Eq. (12) becomes,

$$\ln \mathcal{Z}_{\beta,\beta\mu} \approx \sum_{A=1}^{\infty} \int \int \frac{d^3 r d^3 p}{h^3} \sum_n g_n(A) \exp [-\beta (e_n(A, \vec{p}) - \mu A)] \quad (13)$$

$$\approx V \left(\frac{mT}{2\pi\hbar^2} \right)^{3/2} \sum_{A=1}^{\infty} A^{3/2} \exp [-\beta (f_{\beta}(A) - \mu A)], \quad (14)$$

where $g_n(A)$ accounts for the degeneracy of internal state (n) , the internal entropy is given by $\exp s(A, e) = \sum_n g_n(A) \delta(e - e_n(A))$, and we have made a saddle point approximation,

$$\int_{-\infty}^{\infty} de \exp [s(A, e) - \beta e] \approx f_{\beta}(A), \quad (15)$$

where the cluster free energy at temperature $T = \beta^{-1}$ is given by $f_{\beta} = \langle e(A) \rangle_{\beta} - T \langle s(A) \rangle_{\beta}$.

It is important to stress that the original Fisher model (Ref. [16]) employs the saddle point approximation Eq. (15), but it does not include translational and internal degrees of freedom. For consistency these latter should be accounted directly in the partition sum Eq. (5), see Eq. (2). If this is done the key expression Eq. (8) is not valid any more, and this is why we include these extra degrees of freedom only at the level of the single-cluster partition sum $\omega_{\beta,\beta\mu}(A)$, leading to the approximation Eq. (13).

For nuclear (fermionic) clusters both the average cluster energy and entropy can be evaluated in the low temperature Fermi gas approximation

$$\langle e(A) \rangle_{\beta} = -B(A) + a_0 A T^2; \quad (16)$$

$$\langle s(A) \rangle_{\beta} = \left(2a_0 T + a_s A^{-1/3} f(T) \right) A - \tau \ln A, \quad (17)$$

and to have an analytically solvable model, the fragment binding energy $B = -e_1$ can be simply parameterized as:

$$B(A) = a_v A - a_s A^{2/3}. \quad (18)$$

The surface term $a_s A^{2/3} f(T)$ in Eq. (17) effectively accounts for the entropy increase at finite temperature due to surface excitations. In particular if we choose for $f(T)$ a smooth function such that $f(T) = \beta$ for $\beta \leq \beta_c$, this naturally produces a vanishing surface free energy at the critical point $\beta_C = T_C^{-1}$. Concerning the Fisher topologic factor $\tau \ln A$, it insures a fragment fractal dimension at the critical point. The physical meaning of this term, as pointed out in Ref. [42], is related to the treatment of the center of mass degree of freedom close to a critical point. In such a situation, the available states for the center of mass motion have to be reduced respect to those of a free particle, and this can be accounted by reducing the exponent associated to the translational energy factor $\propto A^{3/2}$ in Eq. (14). We have taken $\tau = \tau_0 + 3/2 = 3.7$ in order to recover the fractal dimension of the LG universality class. A more sophisticated temperature dependent expression for τ has been proposed in Ref. [42].

The specific form of Eqs. (17) and (16) insures that the model is critical at $T = T_C$, $\mu = \mu_C = -a_v - a_0 T_C^2$. Indeed, computing the average multiplicity of clusters of size A ,

$$\begin{aligned} \langle n_A \rangle_{\beta, \beta\mu} &= \frac{\partial \ln \mathcal{Z}_{\beta\mu}}{\partial (\beta\mu)} \equiv \omega_{\beta, \beta\mu}(A) = \\ &= V \left(\frac{mT}{2\pi\hbar^2} \right)^{3/2} A^{3/2} \exp[-\beta(f_\beta(A) - \mu A)]. \end{aligned} \quad (19)$$

One can see that the partition sum of the Fisher model is simply given by the sum of all the possible cluster multiplicities:

$$\ln \mathcal{Z}_{\beta, \beta\mu} = \sum_{A=1}^{\infty} \langle n_A \rangle_{\beta, \beta\mu}. \quad (20)$$

At $T = T_C$, $\mu = \mu_C$ the fragment multiplicity obeys a power law,

$$\langle n_A \rangle_{\beta_C, \beta_C \mu_C} = V \left(\frac{mT_C}{2\pi\hbar^2} \right)^{3/2} A^{-\tau_0}. \quad (21)$$

Since the different thermodynamic observables can be expressed as successive derivatives of the partition sum, this means that all thermodynamic quantities will exhibit a power law behavior at the approach of $T = T_C$, $\mu = \mu_C$. In particular the critical exponents γ , α may be calculated numerically out of the total particle number,

$$\begin{aligned} \chi &\propto |T_C - T|^{-\gamma}, \\ &= \frac{\sigma_{N; \beta, \beta\mu}^2}{T} = \frac{1}{T} \frac{\partial^2 \ln \mathcal{Z}_{\beta, \beta\mu}}{\partial \alpha^2}, \end{aligned} \quad (22)$$

and, respectively, total energy fluctuation,

$$\begin{aligned} C_V &\propto |T_C - T|^{-\alpha}, \\ &= \frac{\sigma_{E; \beta, \beta\mu}^2}{T^2} = \frac{1}{T^2} \frac{\partial^2 \ln \mathcal{Z}_{\beta, \beta\mu}}{\partial \beta^2}. \end{aligned} \quad (23)$$

It is easy to see that any value for the topologic exponent $2 < \tau_0 < 3$ will produce a diverging susceptibility χ and a finite critical density,

$$\rho_c = \frac{1}{\tau_0 - 2} \left(\frac{mT_C}{2\pi\hbar^2} \right)^{3/2}, \quad (24)$$

The critical pressure is also immediately calculated as,

$$P_C = T_C \frac{\ln \mathcal{Z}_{\beta, \beta\mu}|_C}{V} = T_C \left(\frac{mT_C}{2\pi\hbar^2} \right)^{3/2} \frac{1}{\tau_0 - 1}. \quad (25)$$

This formulation together with its canonical and microcanonical counterparts have been extensively used to study nuclear multifragmentation and most of the interesting features of its associated thermodynamics [43, 44, 45, 46]: phase transition, critical behavior, finite size, isospin asymmetry and Coulomb effects, often with contradictory results.

B. The Metropolis Monte-Carlo approach

A complementary way to solve our problem is by employing a Metropolis Monte-Carlo investigation of the configuration space. While having the obvious disadvantage of being analytically non-tractable, this method has the advantage of being solvable without approximations for any finite number of particles. Let us start again from the grand-canonical partition sum of the cluster model for a finite system of volume V :

$$\mathcal{Z}_{\beta, \beta\mu} = \sum_{(k)} \frac{1}{N_k!} \int \frac{d^3r_1 \dots d^3r_{N_k} d^3p_1 \dots d^3p_{N_k}}{h^{3N_k}} \exp \left[-\beta \left(E_{tot}^{(k)} - \mu A_{tot}^{(k)} \right) \right], \quad (26)$$

with

$$E_{tot}^{(k)} = \sum_{i=1}^{N_k} e(A_i, \vec{p}_i, n_i); \quad (27)$$

$$A_{tot}^{(k)} = \sum_{i=1}^{N_k} A_i, \quad (28)$$

where again the cluster energy functional consists of kinetic energy and internal levels: $e(A, \vec{p}, n) = e_n(A) + p^2/2Am$. Calculating the phase space integral Eq. (26) simplifies to

$$\begin{aligned} \mathcal{Z}_{\beta, \beta\mu} &= \sum_{(k)} W_k \\ &= \sum_{(k)} \frac{1}{N_k!} V^{N_k} \prod_{i=1}^{N_k} \left(\frac{mA_i T}{2\pi\hbar^2} \right)^{3/2} \exp \left[-\beta (f_\beta(A_i) - \mu A_i) \right], \end{aligned} \quad (29)$$

where we can take the same free energy functional Eqs. (16, 17) as for the Fisher model in order to compare the two approaches. In principle inter-fragment interactions should be taken into account in the form of an excluded volume [32]. This effect is not accounted in the original Fisher model [16] because it is a size-dependent effect which becomes negligible in the thermodynamic limit of interest here, as we will discuss in the next section. Therefore we will consider point-like particles also in the Monte-Carlo version of the model, Eq. (29).

In the thermodynamic limit we can write

$$\lim_{V \rightarrow \infty} \sum_{(k)} \prod_{i=1}^{N_k} = \prod_{A=1}^{\infty} \sum_{n_A=0}^{\infty}. \quad (30)$$

This means that, in the absence of the factorials $1/N_k!$ in Eq. (29) and $1/n_A!$ in Eq. (11), the analytical and Monte-Carlo model would be equivalent at the thermodynamic limit. Because of the factorials, this equivalence is violated: considering the exact counting of all the possible configurations including their translational and internal degrees of freedom breaks the independence of the different cluster sizes Eq. (8) even if we keep the Fisher hypothesis of non-interacting point-like clusters. Eq. (20) has then to be considered as an approximation of the exact partition sum of the cluster model in the thermodynamic limit. The thermodynamic properties of the cluster model should then be investigated solving numerically Eq. (29) for a finite size system big enough that the independence of the system size is achieved, or that converging quantities can be extracted through finite size scaling techniques.

The spanning of the available configurations in Eq. (29) is done by proposing successively trial configurations which are accepted according to the detailed balance principle:

$$N_k! P(k \rightarrow k') W_k \Delta k = N_{k'}! P(k' \rightarrow k) W'_k \Delta k', \quad (31)$$

see Ref. [32] for details. Direct access to full thermodynamical information of each statistical configuration allows one to trace phase coexistence from the bimodal structure of the different probability density distributions [47, 48] and, moreover, to identify to which phase each configuration belongs.

In general and by construction, the double peak structure of the probability distribution originates from the convex intruder in the surface of the associated density of states as a function of the order parameter of the underlying first-order phase transition[47]. We expect particle and energy density as possible order parameters. In the grand-canonical

case under consideration, the probability distribution in the presence of a first order phase transition should then be double-peaked with respect to the extensive observables A_{tot} and E_{tot} conjugated to the Lagrange multipliers β and $\alpha = \beta\mu$.

To allow for a straightforward comparison with the case of nuclear matter, in this Section, the following set of parameters will be used: ($a_v=16$ MeV, $a_s=16$ MeV, $a_0=1/16$ MeV $^{-1}$, $T_c=16$ MeV). To test the results stability to model parameters, two different expressions have been employed for $f(T)$:

- (i) $f(T) = T^{-1} \left[1 - \left((T_C^2 - T^2)/(T_C^2 + T^2) \right)^{1.25} \Theta(T_C - T) \right]$, and
- (ii) $f(T) = T^{-1} [1 - (1 - T/T_C) \Theta(T_C - T)]$.

C. The phase diagram

Let us consider a system confined into the finite volume V and denote by A_0 the maximum number of particles corresponding to normal density, $\rho_0 = A_0/V$.

Fig. 1 illustrates the probability distributions of the total number of particles (left panel) and total energy (right panel) for a system characterized by $V=14476.4$ fm 3 ($A_0=2000$) at different values of (β, α) , together with the phase diagram (stars) in temperature - total density (left) and temperature - total energy (right) representations. To allow superposition of the above plots, the normalization factors of the probability distributions have been arbitrarily altered such that the peak heights correspond to the coexistence temperature represented on the left Y-axis. To estimate finite size effects, the phase diagram of a system two times smaller ($V=7238.2$ fm 3 and $A_0=1000$) is represented with open squares.

Given that A_{tot} and E_{tot} are correlated, at the thermodynamic limit the phase-coexistence information provided by the bimodal structure of the these distributions should be the same. Indeed, the phase-coexistence temperature - defined by the temperature value for which the peaks belonging to the dense and diluted phases have the same height if α is kept constant, differs by less than 0.1 MeV when one considers $Y(A_{tot})$ or $Y(E_{tot})$ distributions. This is coherent with a one-dimensional order parameter transition like ordinary liquid-gas.

It is interesting to observe that correct thermodynamic information is obtained also from the probability distributions of the largest cluster A_{max} in each event (middle panel) as in fragmentation transitions. This is due to the strong correlation of A_{max} with the total energy deposit [49, 50, 51]. Even more interesting, plotted as a function of $(1 - A_{max}/A_0)$, the phase diagram built out of A_{max} bimodality sits perfectly on the top of the one built analyzing the bimodality of $Y(A_{tot})$ distributions. Thus, we confirm that A_{max} is a good order parameter in the cluster model. This is an encouraging result for the experimental search of the finite nuclei phase diagram out of the measured A_{max} distributions [27, 28].

As one may see in Fig. 1, the shape of the phase diagram does not depend on the system size. The gas-like branch approaches the critical point of the analytical Fisher model discussed in the previous section. However, the limiting point characterized by $T_{lim}=16$ MeV and $\alpha_{lim}=-2$, where by construction the fragment size distribution is an exact power law, lies on the line $\rho = \rho_0$, which is very different from the value $\rho_c \approx 0.07488$ fm $^{-3}$ obtained in the analytical Fisher model Eq. (24). The same result has been obtained in Ref. [46], where the phase diagram of a 1-component clusterized system was calculated analytically out of the Gibbs equations. This result is not physical and is due to the fact that the cluster model considers all nuclear clusters fully incompressible, including the asymptotic limit of nuclear matter.

Within this modelisation, the shape of the phase diagram and in particular its limiting temperature are independent of the system size for any $A_0 > 100$. This means that the thermodynamic limit may be addressed directly from finite size systems calculations without performing finite size scaling. Finite size scaling implies a power law for the size dependence of the limiting temperature if this latter corresponds to a critical point, according to

$$(T_{lim}(L) - T_C) \propto L^{-1/\nu}, \quad (32)$$

where L is the system linear dimension, $T_C = \lim_{L \rightarrow \infty} T_{lim}(L)$, and ν is the critical exponent related to the divergence of the correlation length at the critical point, $\xi \propto |1 - T/T_C|^{-\nu}$. The observed independence of $T_{lim}(L)$ from the system size indicates that the correlation length of the infinite system does not diverge at T_C , which means that the limiting point is not a critical point. This again is at variance with the results of the analytical Fisher model, and in contradiction with most expectations on nuclear multifragmentation based on statistical clusters models.

Before leaving this section, we mention that the shape of the phase diagram proves insensitive to the functional dependence according to which the surface energy term vanishes while approaching T_C . The solid stars and open squares in Fig. 1 correspond to the case in which $f(T)$ has the form (i).

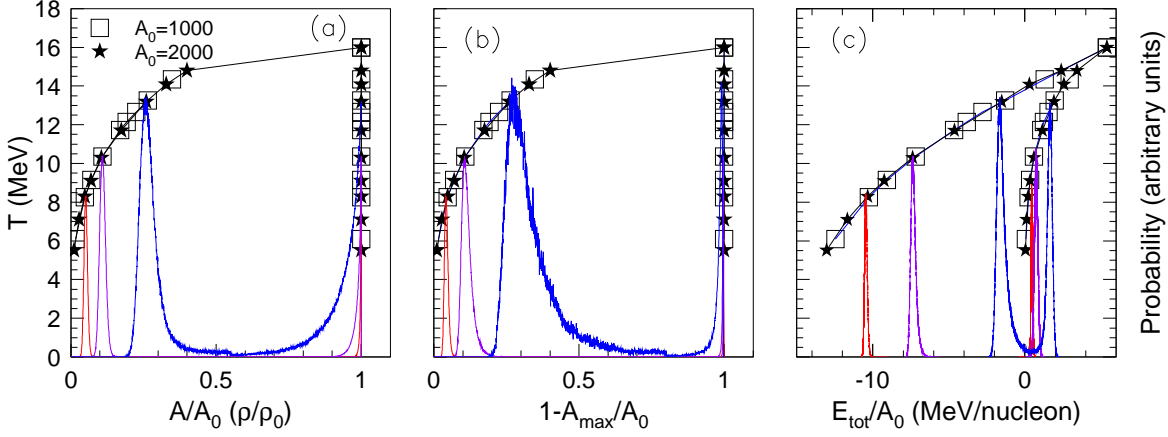


FIG. 1: (color online) Probability distributions of the total number of particles (left), largest fragment in each event (middle) and total energy (right) for a one-component cluster model with standard Fisher fragment definition in the grand-canonical ensemble characterized by $V=14476.4 \text{ fm}^3$ ($A_0=2000$) and $(T, (\mu/T)) = (8.3, -2.40)$, $(10.35, -2.20)$ and $(13.19, -2.05)$, where T is expressed in MeV (Metropolis simulation results). The normalization factors are chosen such that the peak heights correspond to the coexistence temperature. The solid star symbols mark the phase diagram in temperature - density (left and middle panel) and temperature - total energy representations as obtained out of the bimodality of corresponding distributions. Open squares mark the phase diagram of a system half the size, ($V=7238.2 \text{ fm}^3$ and $A_0=1000$).

D. Criticality

The question whether or not this second-order transition point is indeed a critical point may be also answered calculating different critical exponents and checking whether they do verify, together with the input τ , the corresponding equality relations [16],

$$\frac{\gamma}{(2-\alpha)} = \frac{(3-\tau)}{(\tau-1)} = 1 - \frac{2\beta}{2-\alpha}, \quad (33)$$

and,

$$\delta = \frac{1}{\tau-2}. \quad (34)$$

The full thermodynamic characterization of the system allows the calculation of β and δ out of the curvature of the coexistence curve,

$$\left(1 - \frac{\rho_{coex}}{\rho_C}\right) \propto \left(1 - \frac{T}{T_C}\right)^\beta, \quad (35)$$

and, respectively, the shape of the critical isotherm,

$$(p_C - p)|_{T_C} \propto (\rho_C - \rho)|_{T_C}^\delta, \quad (36)$$

which is equivalent through $(p_C - p) \propto \rho_C(\mu_C - \mu)$ to,

$$(\mu_C - \mu)|_{T_C} \propto (\rho_C - \rho)|_{T_C}^\delta. \quad (37)$$

The absence of finite size effects in the phase diagram allows direct extraction of β out of the curvature of the coexistence curve, Eq. (35). The results of the Metropolis simulation for the one-component clusterized system in the grandcanonical ensemble are plotted in panel (a) of Fig. 2 with solid stars along with the predictions of the analytical model, represented with open circles. Over the explored (μ/T) domain the coexistence curve ρ_{coex} exhibits the expected power law behavior as a function of T in the two models, with slightly different values for the exponents.

By contrast with this, when approaching the critical point the critical isotherm deviates from the expected linear behavior and the magnitude of these deviations increases with the system size, as illustrated in the panel (b) of Fig. 2 where full and open stars correspond to the predictions of the grandcanonical one-component Metropolis model with $A_0=2000$ and 4000. This behavior can be understood taking into account that the calculation of ρ demands the evaluation of the average number of particles, a quantity which, like any statistical average, is naturally affected by the finite size of the system. The slope of the linear region $\delta=5.2$ is, nevertheless, fairly close to the predictions of the analytical model such that one may conclude that the hyperscaling equation (34) holds.

γ and α may be directly extracted out of the fluctuations of the system total energy and total number of particles via Eqs. (22) and (23) along the critical $\alpha=-2$ path.

The results of the Fisher analytical model shown in panels (c,d) fulfill again perfectly the hyperscaling relations Eq. (33), as expected from the discussion of the previous section. Since fluctuations should diverge at the approach of a critical point, the Monte-Carlo results obtained for a finite system must obviously saturate at a finite value.

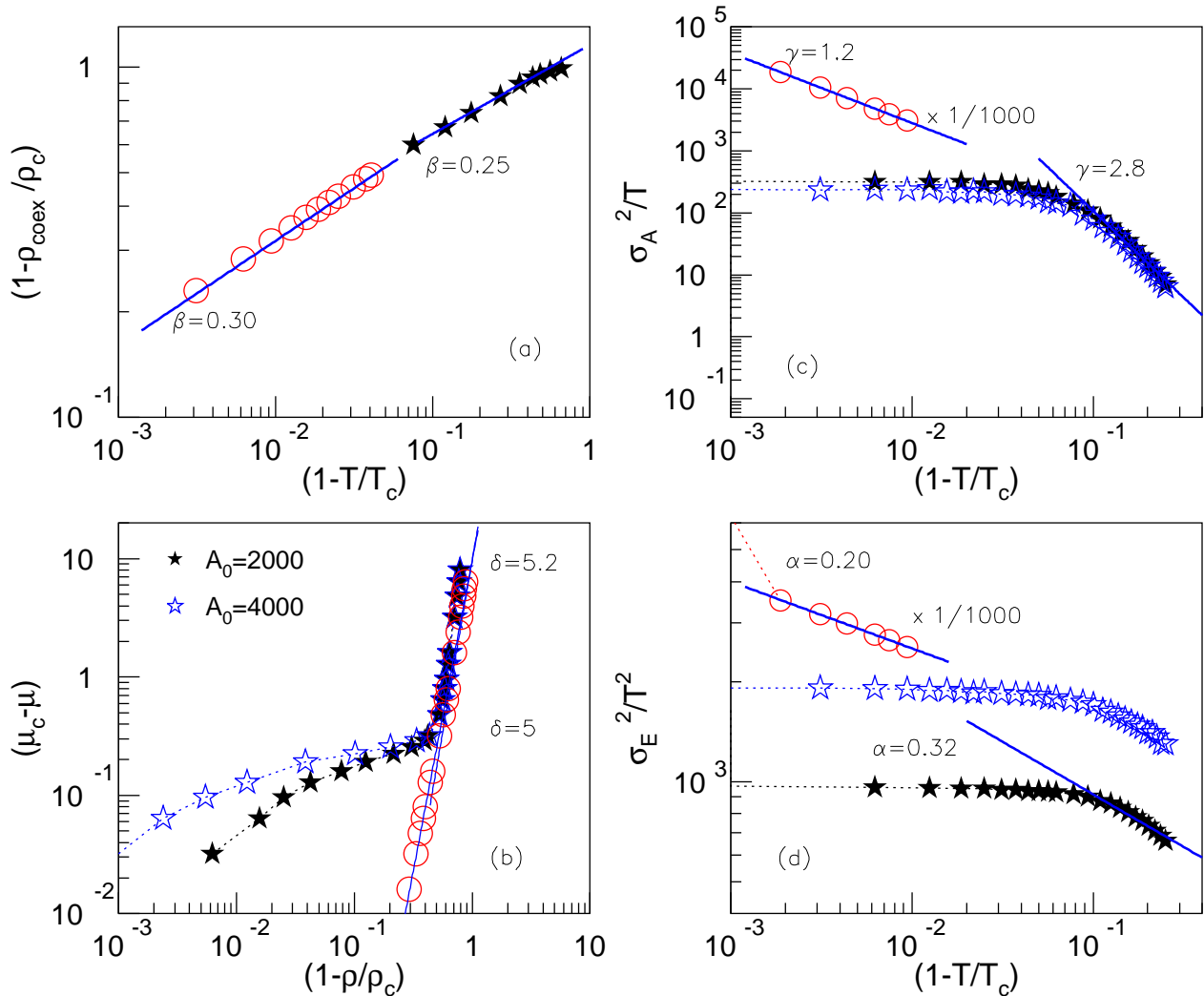


FIG. 2: (color online) Extraction of critical exponents corresponding to a one-component clusterized system within a grand-canonical ensemble out of the thermodynamical properties. Results corresponding to the analytical model are plotted with open circles, while stars stand for the results of the Metropolis simulation. In this last case, the maximum number of particles allowed by the fixed volume in $A_0 = 2000$ (solid stars) and, respectively, $A_0 = 4000$ (open stars). Panel a: β extracted out of the coexistence curve $\rho - T$; panel b: δ extracted out of the critical isotherm; panel c: γ extracted out of total particle number fluctuations; panel d: α extracted out of total energy fluctuations. Cases (c) and (d) consider the critical (μ/T) path.

TABLE I: Critical exponents for a one component clusterized system within a grandcanonical ensemble as obtained from a Metropolis simulation in comparison with results of the analytical model.

Critical exponent	Calculation method	Monte Carlo	Analytical	Theoretical
α	$\sigma_E^2/T^2 \propto T - T_C ^{-\alpha}$	0.34	0.2	0.2
γ	$\sigma_A^2/T \propto T - T_C ^{-\gamma}$	2.8	1.2	1.2
β	$(\rho_C - \rho_{coex}) \propto (T_C - T)^\beta$	0.25	0.33	0.33
δ	$(p_C - p) _{T_C} \propto (\rho_C - \rho) _{T_C}^\delta$	5.2	5	5
γ_{fr}	$m_2 \propto (T_C - T)^{-\gamma}$	2.8		1.2
β_{fr}	$A_{max} \propto (T_C - T)^\beta$	0.33		0.33
$(\beta/\gamma)_{fr}$	$A_{max} \propto S_2^{\beta/\gamma}$	0.16	0.275	0.275

This can be seen in panels c and d, where, irrespective of the system size, one may distinguish two regimes for the Monte-Carlo results: in the temperature domain $0.1 < 1 - T/T_C < 0.7$, σ_A^2/T and σ_E^2/T^2 are linear with a non-null slope, while for T approaching T_C , the two curves get flat. The comparative analyze of $A_0=2000$ and 4000 results shows that neither the widths of the two intervals, neither the value of the non-null slope depend on the system size. The first observation is a first indication that the system might not be critical. Indeed, if the system were critical, by increasing the system size, the linearity domain close to the critical point would increase. This is obviously not the case here. The second observation is in line with the lack of system size dependence in the phase diagram and allows one to extract the critical exponents without performing finite size scaling. The values $\alpha = 0.34$ and $\gamma = 2.8$ obtained over the region where $\ln(1 - \rho_{coex}/\rho_C)$ vs. $\ln(1 - T/T_C)$ is linear are so different from the expected values $\alpha = 0.2, \gamma = 1.2$ extracted from Eq. (33) that it is difficult to believe that this can be a finite size effect.

The ensemble of these results show that criticality is violated in the cluster model even if the surface tension vanishes at the limiting point of the first-order phase transition.

In percolation theory over infinite [52] and small lattices [53], critical exponents may be extracted from k -moments of the cluster distributions,

$$m_1 = \sum_s s n(s) \propto (p - p_C)^\beta, \quad (38)$$

$$m_2 = \sum_s s^2 n(s) \propto |p - p_C|^{-\gamma}, \quad (39)$$

where p , the probability that a lattice site is occupied, is the control parameter. When dealing with finite systems at $T < T_C$, the largest cluster assimilated with the liquid phase must be excluded from summations [52].

In nuclear multifragmentation, and Eqs. (38) and (39) have been employed in the equivalent forms [17, 18]

$$A_{max} \propto (T_C - T)^\beta, \quad \text{for } T < T_C, \quad (40)$$

$$m_2 \propto (T_C - T)^{-\gamma}, \quad \text{for } T < T_C, \quad (41)$$

and,

$$A_{max} \propto S_2^{\beta/\gamma}, \quad (42)$$

where $S_2 = m_2/m_1$, and often the distance to the critical point $T - T_C$ has been estimated from the fragment multiplicity M . Eq. (42) is particularly easy to handle as it does not require data sorting according to T , a quantity very difficult to infer experimentally.

Fig. 3 investigates to what extent the parallelism between percolation on lattice and clusterized matter holds. The evolution of the second moment of the cluster distribution and the largest fragment in each event as a function of $(1 - T/T_C)$ for $T < T_C$ are plotted along the critical $\alpha=-2$ path (panels a and b). After eliminating the region where divergences are rounded-off by finite size effects, one gets $\gamma_{fr} = 2.8$ and $\beta_{fr}=0.33$. The result for γ is in excellent agreement with the fluctuation estimation, and again very different from the value $\gamma = 1.2$ one should get to have thermodynamically consistent exponents. The slight disagreement between the β values may be surprising

considering that we have observed that A_{max} is an excellent order parameter in the cluster model. However it is interesting to note that, at variance with all other procedures here employed, Eq. (40) proves sensitive to the way in which fragment surface energy vanishes while approaching the limiting temperature. For instance for $f(T) = T^{-1} [1 - (1 - T/T_C) \Theta(T_C - T)]$, Eq. (40) leads to $\beta_{fr}=0.25$. The predictions of Eq. (42) are illustrated in panel c for $12 \text{ MeV} < T < 24 \text{ MeV}$ along $\alpha=-2$. Liquid-like and gas-like branches of the Campi plot give $(\beta/\gamma)_{fr}=0.16$. This number is not compatible with criticality which would require $(\beta/\gamma) = 0.275$, but it is in striking agreement with the values reported in the experimental multifragmentation literature [17, 20]. This result is surprising since deviations might have been expected in data due to the Coulomb interaction.

Before leaving this section let us mention that, if we would only dispose of cluster observables as in the experimental case of multifragmentation, the results for $(\beta/\gamma)_{fr}$, γ_{fr} and β_{fr} from Eqs. (40), (41) and (42), would make us erroneously conclude that the exponents are thermodynamically consistent and the system is critical.

The values of the above discussed critical exponents are summarized in Table I together with the employed equations.

E. Temperature dependent bulk energy

In this study we have always considered completely incompressible fragments. In this section we focus on what happens to the thermodynamics of a one-component clusterized system if, in addition to a_s , also a_v vanishes while approaching T_C . From the physical point of view, no microscopic calculation suggests that this can be the case, however this simplified calculation may give a glimpse on what could happen if compressibility effects were realistically introduced, leading to a reduced bulk energy at finite temperature. The phase diagram obtained as described in Sec. IIC is represented in Fig. 4 with solid circles. Same symbols are used in Figs. 5 and 6 to depict the evolution of different thermodynamical and fragment observables out of which critical exponents are calculated as described in Sec. IID.

The first result is that, when plotted in $T - \rho$, the phase diagram superimposes perfectly on the top of the one corresponding to standard fragment definition. This is however not valid in $T - E$ representation, because of the different fragment energetics and, moreover, $(\mu/T)_C=0$. The stability of the $T - \rho$ phase coexistence borders suggests that the critical exponents β and δ extracted out of the curvature of phase coexistence and shape of the critical isotherm have the same values as before. The confirmation is given in Fig. 5, panels a and b. Panel d shows that neither the divergence of $\ln(\sigma_E^2/T^2)$ vs. $\ln(1 - T/T_C)$ is affected. By contrast, $\ln(\sigma_A^2/T)$ vs. $\ln(1 - T/T_C)$ gets a linear dependence over a broader region and $\gamma=1.9$. Hyperscaling relations are still violated and critical behavior does not hold. Fig. 6 shows that critical exponents extracted out of fragment properties are in reasonable agreement with the values calculated from the thermodynamic behavior. In this case, $f(T) = T^{-1} [1 - (1 - T/T_C) \Theta(T_C - T)]$.

III. APPLICATION TO FINITE SYSTEMS - SENSITIVITY TO THE STATISTICAL ENSEMBLE

As we have already mentioned, Fisher cluster models have been intensively used to address multifragmentation [43, 44, 45] and the thermodynamic behavior of finite systems has been constantly compared to the one of their infinite counterparts. The long-range non-saturating Coulomb interaction, which has to be included when describing finite fragmenting nuclei, prevents addressing the thermodynamic limit and will not be considered here. Interference with isospin-asymmetry effects is also avoided by exclusively considering isospin-symmetric systems. Even if we ignore these effects, realistic applications to fragmenting finite nuclear systems differ from the model we have presented in Section II also because they take into account the excluded volume correction to the translational motion and do not generally consider the topologic Fisher factor.

These differences suggest that the multifragmentation phase diagram may be different from the one plotted in Fig. 1.

To see whether it is the case, the phase diagrams of different charge-neutral isospin-symmetric systems ($A_0=200$, 500, 3600) obtained as described in Section IIC are depicted in Fig. 7 with open circles, open stars and, respectively, solid circles. Standard nuclear multifragmentation fragment definition is employed [32]. Parameters of fragment binding energy have values close to the one used in Section II, $a_v=15.4941$, $a_s=17.9439$, and we have additionally taken for the symmetry energy $a_I = 1.7826$ [54]. Nuclear level density is taken as,

$$\rho(\epsilon) = \frac{\sqrt{\pi}}{12a^{1/4}\epsilon^{5/4}} \exp(2\sqrt{a\epsilon}) \exp(-\epsilon/\tau), \quad (43)$$

with $a = 0.114A + 0.098A^{2/3} \text{ MeV}^{-1}$ and $\tau=9 \text{ MeV}$ [55].

As one may notice, the liquid border of the coexistence zone is stable at $\rho = \rho_0$, but the temperature of the second-order transition point is situated well below $T_C=16$ MeV and, moreover, presents a system size dependence. The shift is essentially due to the factor $A^{3/2}$ in the partition sum coming from the translational motion which does not vanish even at T_C . In this case, it is clear that not only critical behavior is lost, but also the power law shape of fragment size distributions in the vicinity of the phase diagram limiting point. This result is in qualitative agreement with the conclusions of Ref. [43], where the translational energy factor in the fragment partition sum is responsible for the diminish of the second-order transition temperature from 16 MeV to 7 MeV and the lost of linear shape of

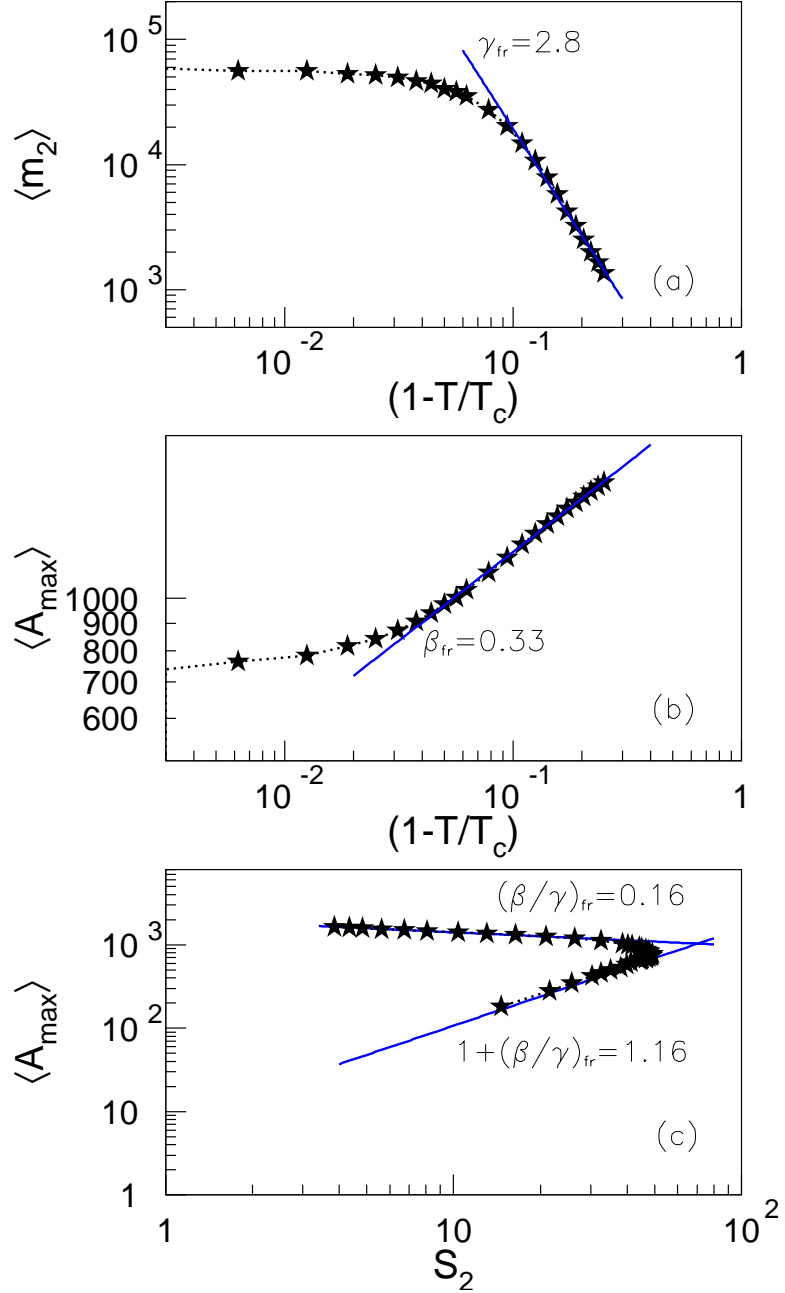


FIG. 3: (color online) Extraction of critical exponents γ (Eq. (39), top panel), β (Eq. (40), middle panel) and β/γ (Eq. (42), bottom panel) out of fragment properties along the critical $(\mu/T)=-2$ path in the case of a one-component clusterized system within a grand-canonical ensemble. The maximum number of particle allowed by the fixed volume in $A_0 = 2000$.

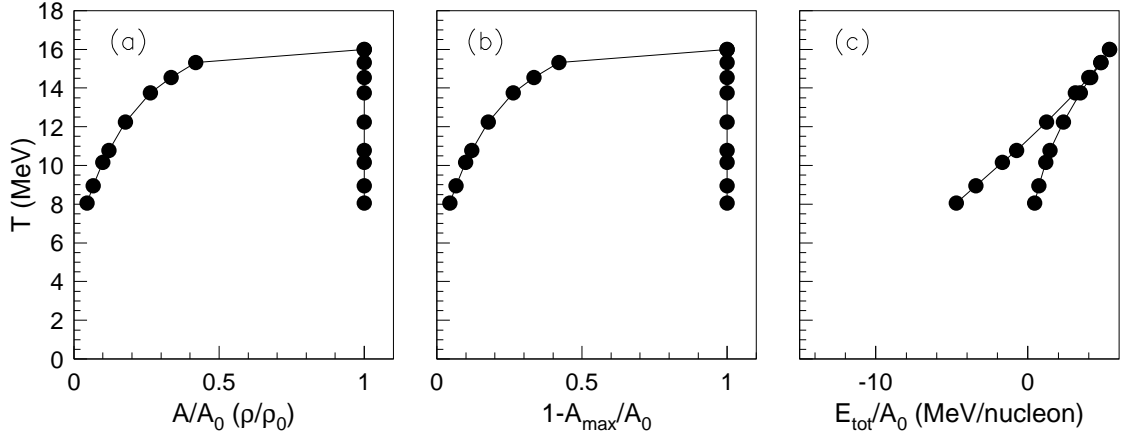


FIG. 4: The phase diagram in temperature - density (left and middle panel) and temperature - total energy representations as obtained out of the bimodality of corresponding distributions for a system characterized by $V=14476.4 \text{ fm}^3$ ($A_0=2000$) within the grand-canonical ensemble. At variance with standard fragment definition, here we assume a temperature dependence of the bulk energy.

fragment size distributions in log-log scale.

The system size dependence of T_{lim} is due to the inclusion of inter-fragment interactions by means of an excluded volume in the spirit of the Van der Waals gas and persists up to $A_0 \approx 4000$.

Indeed, if we consider that only the space not occupied by the clusters is available for the center-of-mass motion, the factor V^{N_k} in Eq. (29) has to be replaced by

$$V(V - V_1)(V - V_1 - V_2) \dots (V - V_1 - V_2 - \dots - V_{N_{k-1}}), \quad (44)$$

where V_i is the volume occupied by cluster i . Assuming for simplicity that $V_1 = V_2 = \dots = V_{N_k} = (V/n)/N_k$, the above expression may be written as $V^{N_k} \xi$ with

$$\xi = \prod_{i=1}^{N_k-1} \left(1 - \frac{i}{nN_k}\right), \quad (45)$$

where $n = V/V_0$, see Ref. [32] for details. Since,

$$\lim_{V \rightarrow \infty, V_0 \rightarrow \infty} \xi = 1, \quad (46)$$

we can see that the excluded volume effect becomes negligible only for very large systems. This confirms that the point-particle approximation is correct when dealing with the thermodynamic limit.

Even more important, the thermodynamics of a finite system depends on the statistical framework in which it is investigated. A constant pressure canonical ensemble may be used to trace $\rho - T$ phase diagrams out of the bimodality of the volume and to immediately compare them with the phase diagrams obtained grandcanonically out of the bimodality of the total number of particles. The results corresponding to two systems ($A=200$ and 1000) are depicted in Fig. 8 with open and solid circles in different representations. As above, the system size dependence of T_{lim} is the consequence of excluded volume corrections. Contrary to the grandcanonical results, in this case the liquid border of the phase coexistence region extends over the whole density domain and the coexistence region at low temperatures shrinks to the vicinity of $\rho = 0$. The limiting point is characterized by $\rho = \rho_0$. As the size of the system increases, the constant-pressure canonical phase diagram approaches the grand-canonical one to which it is identical in the thermodynamic limit. The convergence is nevertheless very slow.

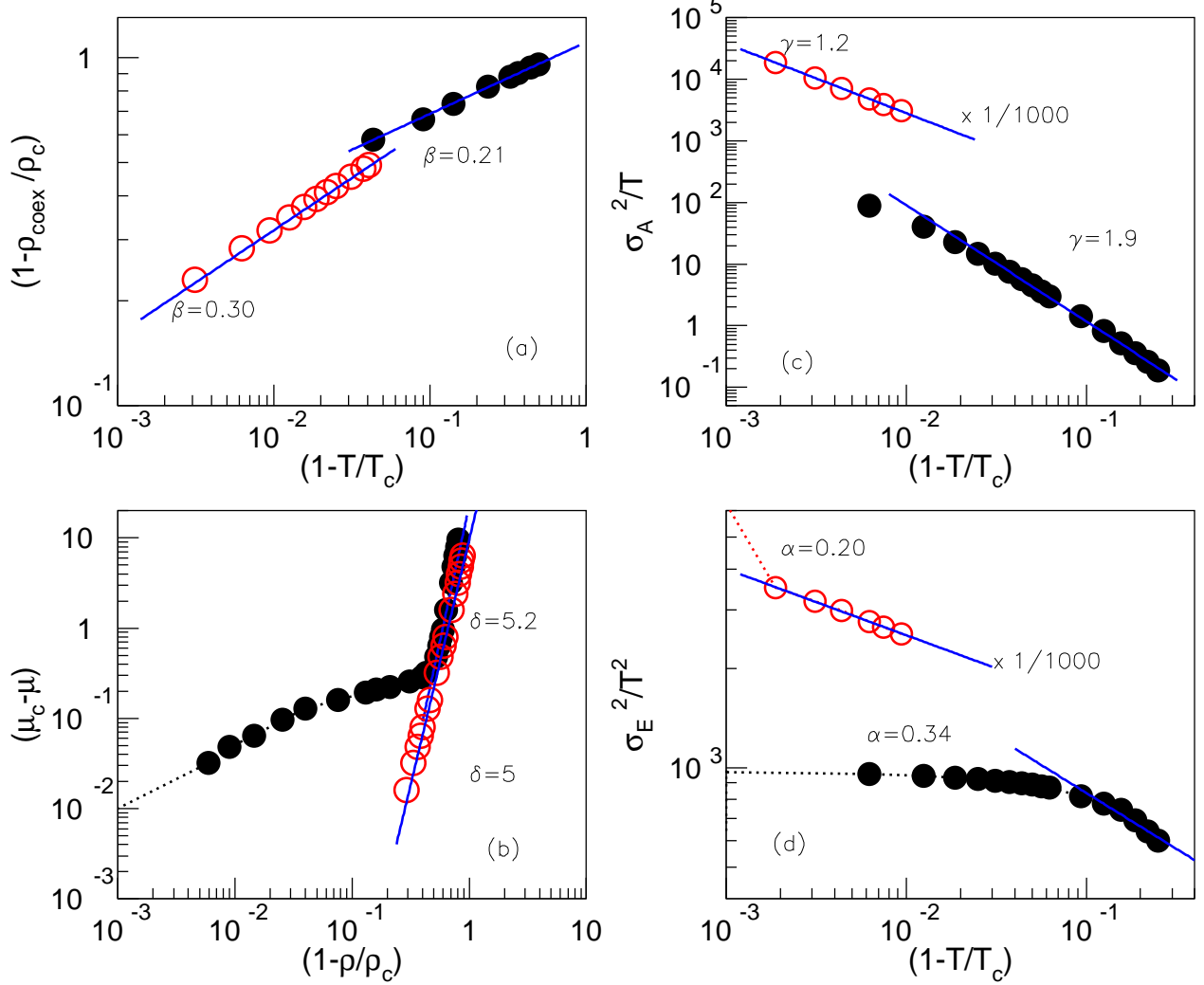


FIG. 5: (color online) The same as in Fig. 2 for the case in which bulk energy depends on temperature. Results of Metropolis calculation (solid circles) correspond to $A_0=2000$.

IV. APPLICATION TO INFINITE SYSTEMS: NEUTRON STARS

Clusterized nuclear matter in the temperature and density domain of a liquid-gas phase transition is predicted to be produced also in the core of supernovae and in the inner crust of neutron stars [6, 7, 8, 9, 10, 11, 12, 13]. In this case, the system's net charge neutrality is insured by the ultra-relativistic gas of electrons in which the nuclear fragments are embedded.

In the free neutron regime ($4.3 \times 10^{11} \text{ g/cm}^3 \leq \rho \leq 2.5 \times 10^{14} \text{ g/cm}^3$) the matter is presently figured-out as a lattice of nuclei immersed in a nucleon and electron gas and theoretically treated as a succession of non-interacting Wigner-Seitz cells [42, 56, 57].

If we adopt this scenario, the thermodynamics of the whole star crust may be investigated analyzing only one such a cell and represents a perfect application of the cluster model. The effect of the Coulomb energy is that of modifying the energy of cluster configuration, and of suppressing the critical behavior of nuclear matter [5]. Because of that last point, we have not included the Fisher topologic factor $-\tau \ln A$ in the cluster entropy. Concerning the modified

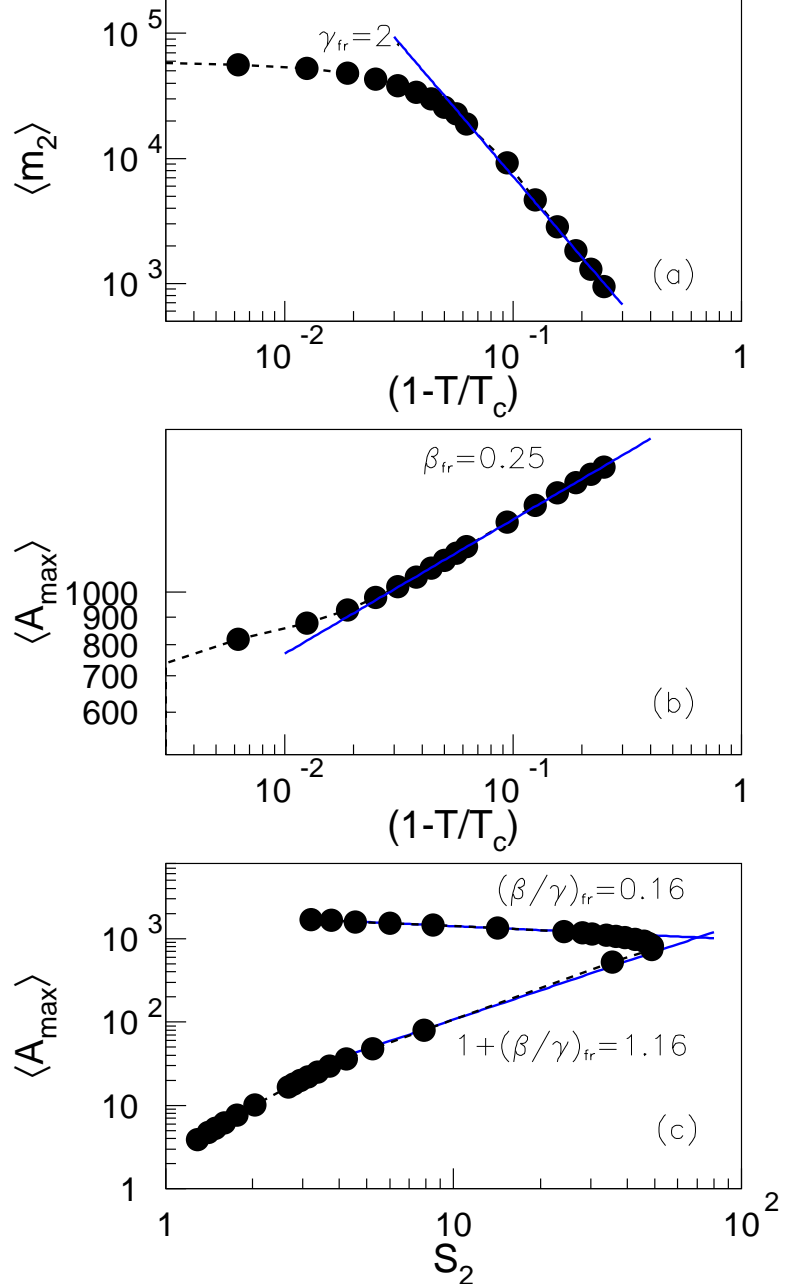


FIG. 6: (color online) The same as in Fig. 3 for the case in which bulk energy depends on temperature. Results of Metropolis calculation are represented with solid circles and $A_0=2000$.

energetics, this effect is taken into account by altering the statistical weight of a configuration Eq. (29) according to,

$$W_k = \frac{1}{N_k!} \exp(-\beta V_C(k)) V^{N_k} \prod_{i=1}^{N_k} \left[\left(\frac{mA_i T}{2\pi\hbar^2} \right)^{3/2} \rho(\epsilon_i) w_{\beta, \mu_n, \mu_p}(A_i, Z_i) \right], \quad (47)$$

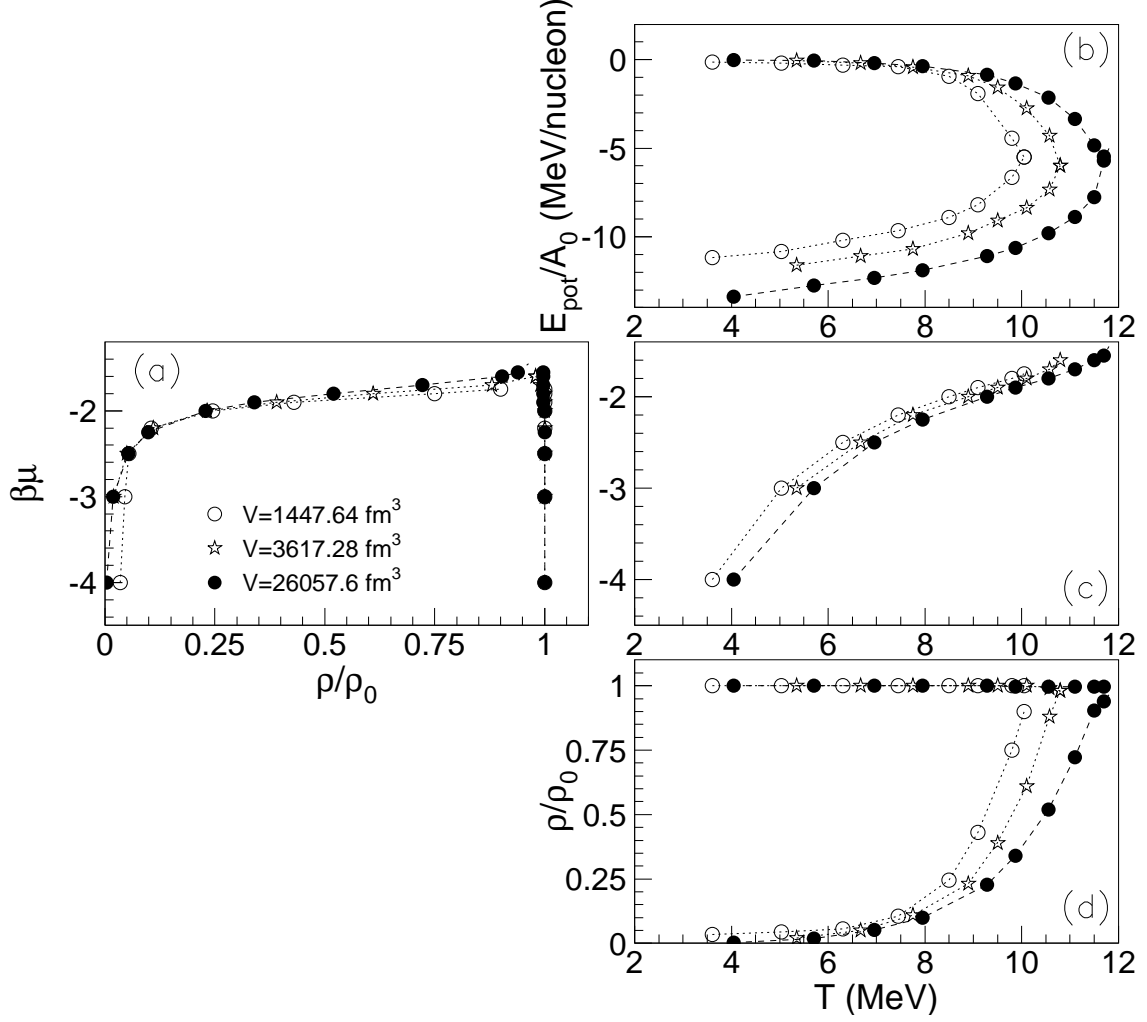


FIG. 7: The phase diagram of the cluster model including excluded volume effects according to Eq. (45) as obtained out of the bimodal behavior of the total number of particles within the grandcanonical ensemble. Left side: $\alpha = \beta\mu$ as a function of density. Right side: potential energy per particle, α and density as a function of temperature. Empty circles, empty stars and solid circles correspond to charge-neutral isospin-symmetric systems with volume $V=1447.64 \text{ fm}^3$ ($A_0 = 200$), $V=3617.28 \text{ fm}^3$ ($A_0 = 500$) and, respectively, $V = 26057.62 \text{ fm}^3$ ($A_0 = 3600$).

where the weight associated to a given cluster (A_i, Z_i) is

$$T \ln w_{\beta, \mu_n, \mu_p}(A_i, Z_i) = \left(a_v A_i - a_s (1 - T f(T)) A_i^{2/3} \right) (1 - a_I (A_i - 2Z_i)^2 / A_i) - \epsilon(A_i, Z_i) + \mu_n (A_i - Z_i) + \mu_p Z_i, \quad (48)$$

and nuclear fragments are described as in Sec. III. The Coulomb energy may be calculated for each configuration as [42],

$$V_C(k) = \sum_{i=1}^{N_k} \frac{3}{5} c(\rho) \frac{e^2 Z_i^2}{r_0 A_i^{1/3}}, \quad (49)$$

with

$$c(\rho) = 1 - \frac{3}{2} \left(\frac{\rho_e}{\rho_{0p}} \right)^{1/3} + \frac{1}{2} \left(\frac{\rho_e}{\rho_{0p}} \right), \quad (50)$$

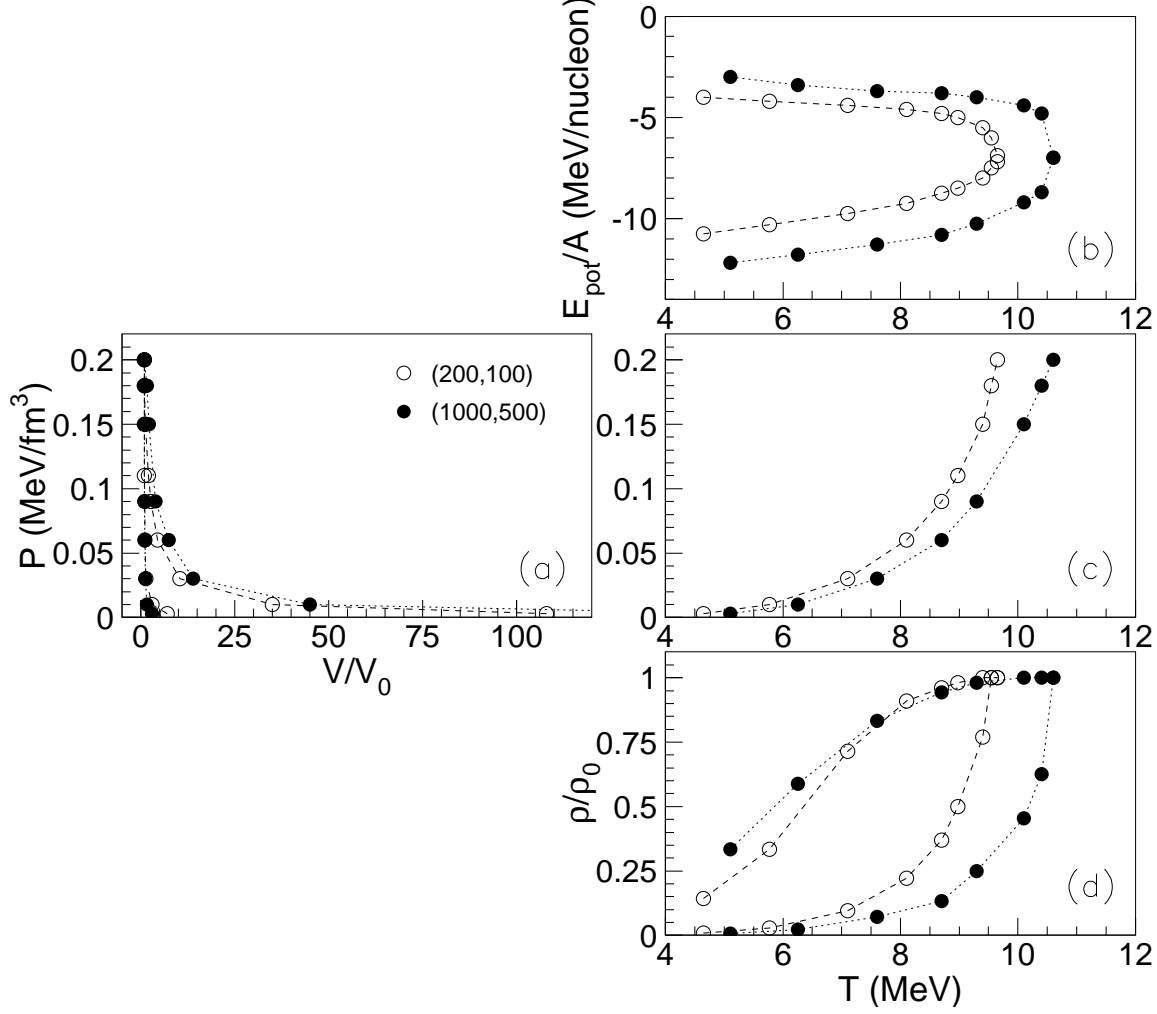


FIG. 8: Phase diagram of the cluster model including excluded volume effects according to Eq. (45) in the isobar canonical ensemble. The considered systems are neutral and isospin-symmetric. Left side: pressure as a function of volume. Right side: potential energy per particle, pressure and density as a function of temperature. Empty circles correspond to a calculation with $A_0 = 200$, filled circles to $A_0 = 1000$.

accounting for the screening effect of electrons. $\rho_{0p} = Z/A\rho_0$ denotes the proton density inside the nuclei and ρ_e is the electron density.

Fig. 9 illustrates the phase diagram of a Wigner-Seitz cell of volume $V=28952.91 \text{ fm}^3$ ($A_0=4000$) as obtained from the bimodality of total particle number distributions in a grandcanonical ensemble.

One may directly compare the obtained phase diagram with the one corresponding to a system of similar size where Coulomb is switched-off (solid symbols in Fig. 7). We can see that the shape of the phase diagram does not change. This would not necessarily be true any more if the weight of the translational motion $\propto (VAT)^{3/2N_k}$ at high temperature was reduced through a temperature dependent reduction factor as in the Lattimer-Swesty equation of state [7]. However the prescription for such a term is completely phenomenological, and we will not employ it here. A clear effect is seen on the limiting temperature, which is diminished by several MeV, in agreement with results obtained in Ref. [34] for small systems. An opposite trend has been obtained within a classical microscopic model for Coulomb frustration [5], and the understanding of this discrepancy requires further analyses.

As observed in section II, the fact that the high density transition line lies along $\rho = \rho_0$ is not physical and is due to the incompressibility assumption of the dense phase which is here represented as a single uncharged nucleus of infinite size. This line cannot therefore be interpreted as a prediction for the crust-core transition density as a function of temperature. Moreover, at densities close to saturation, exotic pasta phases are known to appear [9, 10, 11, 12, 13]

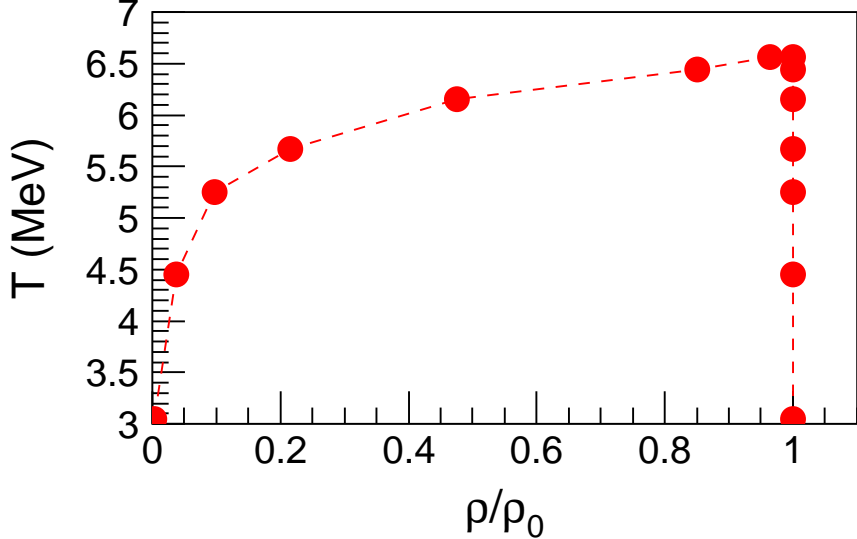


FIG. 9: (color online) Grand-canonical phase diagrams in temperature - density representation for a Wigner-Seitz cell of volume $V=28952.91 \text{ fm}^3$.

and the cluster energy functional should be modified to account for these non-spherical geometries. However in the low density region this model should give a good approximation of the thermodynamics of proto-neutron stars and supernova matter [2, 4, 8]. The evaluation of the equation of state with the inclusion of gammas and neutrinos is in progress.

V. CONCLUSIONS

In conclusion, the thermodynamics of clusterized matter was investigated in connection with a liquid-gas phase transition in nuclear matter. The phase diagram presents first and second order phase transitions and may be derived out of the grand-canonical bimodality structure of total particle number, total energy and largest cluster in each event. Results of an exact Metropolis simulation are systematically compared with predictions of the analytical Fisher model which by construction is critical. At variance with the analytical counterpart, the predictions of the exact model indicate that the liquid phase is characterized by $\rho = \rho_0$ and that vanishing fragment surface energy is not a sufficient condition to obtain criticality.

The clusterized system model is applied to charge-neutral isospin-symmetric finite systems and special attention is given to the way in which the system thermodynamics depends on the employed statistical framework. Clusterized systems with net charge neutrality may be used also to mimic star matter. A first schematic calculation of the phase diagram in the Wigner-Seitz cell approximation is built and it is shown that within this approximation charge fluctuations lead to the decrease of the limiting temperature.

ACKNOWLEDGEMENTS

Ad. R. R acknowledges partial support from the Romanian National Authority for Scientific Research under PNCDI2 programme, grant *IDEI nr. 267/2007* and kind hospitality from LPC-Caen within IFIN-IN2P3 agreement nr. 07-44.

[1] K. Binder, *Physica A* **319**, 99 (2003).

[2] C. Ishizuka, A. Ohnishi and K. Sumiyoshi, *Nucl. Phys. A* **723**, 517 (2003).

[3] H. Sonoda, G. Watanabe, K. Sato, K. Yasuoka and T. Ebisuzaki, *Phys. Rev. C* **77**, 035806 (2008).

[4] A. S. Botvina, I. N. Mishustin, arXiv:0811.2593[astro-ph].

[5] P. Napolitani, Ph. Chomaz, F. Gulminelli and K. H. O. Hasnaoui, *Phys. Rev. Lett.* **98**, 131102 (2007).

[6] D. G. Ravenhall, C. J. Pethick and J. R. Wilson, *Phys. Rev. Lett.* **50**, 2066 (1983).

[7] J. M. Lattimer and M. Prakash, *Phys. Rep.* **333**, 121 (2000).

[8] J. M. Lattimer, F. D. Swesty, *Nucl. Phys.* **A535**, 331 (1991).

[9] G. Watanabe, T. Maruyama, K. Sato, K. Yasuoka and T. Ebisuzaki, *Phys. Rev. Lett.* **94**, 031101 (2005).

[10] C. J. Horowitz, D. K. Berry, *Phys. Rev. C* **78**, 035806 (2008).

[11] W. G. Newton, *Phys. Part. Nucl.* **39**, 1173 (2008).

[12] T. Maruyama *et al.*, arXiv:0901.2622[astro-ph].

[13] S. S. Avancini *et al.*, arXiv:0812.3170[astro-ph].

[14] J. E. Finn *et al.*, *Phys. Rev. Lett.* **49**, 1321 (1982).

[15] H. Jaqaman, A. Z. Mekjian and L. Zamick, *Phys. Rev. C* **27**, 2782 (1983).

[16] M. E. Fisher, *Physics* **3**, 255 (1967).

[17] X. Campi, *J. Phys. A* **19**, L917 (1986); X. Campi, *Phys. Lett.* **B208**, 351 (1988).

[18] M. L. Gilkes *et al.*, *Phys. Rev. Lett.* **73**, 1590 (1994);

[19] J. B. Elliott *et al.*, *Phys. Rev. Lett.* **88**, 042701 (2002).

[20] M. D'Agostino *et al.*, *Nucl. Phys.* **A650**, 329 (1999); *ibid.* *Nucl. Phys.* **A724**, 455 (2003).

[21] Y. G. Ma *et al.*, *Phys. Rev. C* **71**, 054606 (2005).

[22] N. Le Neindre *et al.*, *Nucl. Phys.* **A795**, 47 (2007).

[23] M. D'Agostino *et al.*, *Nucl. Phys.* **A699**, 795 (2002); *ibid.* *Nucl. Phys.* **A734**, 512 (2004).

[24] N. Le Neindre *et al.*, *Nucl. Phys.* **A795**, 47 (2007).

[25] J. D. Frankland *et al.*, *Phys. Rev. C* **71** 034607, (2005).

[26] G. Tabacaru *et al.*, *Eur. Phys. J.* **A18**, 103 (2003).

[27] M. Pichon *et al.*, *Nucl. Phys.* **A749**, 93 (2005); E. Bonnet *et al.*, *Nucl. Phys.* **A816**, 1 (2009) and arXiv:0812.1871[nucl-ex].

[28] M. Bruno *et al.*, *Nucl. Phys.* **A807**, 48 (2008).

[29] D. H. E. Gross, *Rep. Progr. Phys.* **53**, 605 (1990).

[30] J. P. Bondorf, A. S. Botvina, A. S. Iljinov, I. N. Mishustin and K. Sneppen, *Phys. Rep.* **257**, 133 (1995).

[31] S. E. Koonin and J. Randrup, *Nucl. Phys. A* **474**, 173 (1987).

[32] Al. H. Raduta and Ad. R. Raduta, *Phys. Rev. C* **55**, 1344 (1997); *ibid.* *Phys. Rev. C* **65**, 054610 (2002).

[33] Al. H. Raduta and Ad. R. Raduta, *Phys. Rev. Lett.* **87**, 202701 (2001).

[34] F. Gulminelli, Ph. Chomaz, Al. H. Raduta and Ad. R. Raduta, *Phys. Rev. Lett.* **91**, 202701 (2003).

[35] Al. H. Raduta, Ad. R. Raduta, Ph. Chomaz and F. Gulminelli, *Phys. Rev. C* **65**, 034606 (2002).

[36] Ph. Chomaz *et al.*, *Phys. Rep.* **389**, 263 (2004).

[37] S. S. Avancini *et al.*, *Phys. Rev. C* **70**, 015203 (2004).

[38] C. J. Pethick, D. G. Ravenhall, C. P. Lorentz, *Nucl. Phys. A* **584**, 675 (1995).

[39] C. Ducoin *et al.*, *Nucl. Phys. A* **809**, 30 (2008).

[40] I. Vidana, A. Polls, *Phys. Lett.* **B666**, 232 (2008).

[41] Jun Xu *et al.*, arXiv:0901.2309 [astro-ph].

[42] J. M. Lattimer, C. J. Pethick, D. G. Ravenhall and D. Q. Lamb, *Nucl. Phys. A* **432**, 646 (1985).

[43] S. Das Gupta and A. Z. Mekjian, *Phys. Rev. C* **57**, 1361 (1998).

[44] P. Bhattacharyya, S. Das Gupta and A. Z. Mekjian, *Phys. Rev. C* **60**, 054616 (1999); C. B. Das, S. Das Gupta, and A. Majumder, *Phys. Rev. C* **65**, 034608 (2002).

[45] G. Chaudhuri, S. Das Gupta, and M. Sutton, *Phys. Rev. B* **74**, 174106 (2006).

[46] K. A. Bugaev, M. I. Gorenstein, I. N. Mishustin, and W. Greiner, *Phys. Rev. C* **62**, 044320 (2000).

[47] K. Binder and D. P. Landau, *Phys. Rev. B* **30**, 1477 (1984).

[48] F. Gulminelli, *Ann. Phys. Fr.* **29**, 6 (2004).

[49] F. Gulminelli and Ph. Chomaz, *Phys. Rev. C* **71**, 054607 (2005).

[50] F. Gulminelli, *Nucl. Phys.* **A791**, 165 (2007).

[51] G. Chaudhuri, S. Das Gupta, F. Gulminelli, *Nucl. Phys.* **A815**, 89 (2009).

[52] D. Stauffer, *Phys. Rep.* **54**, 1 (1974).

[53] J. B. Elliott *et al.*, *Phys. Rev. C* **49**, 3185 (1994).

[54] G. Audi and A. H. Wapstra, *Nucl. Phys.* **A595**, 409 (1995).

[55] A. S. Iljinov, *et al.*, *Nucl. Phys.* **A543**, 517 (1992).

[56] G. Baym, H. A. Bethe and C. J. Pethick, *Nucl. Phys.* **A175**, 225 (1971).

[57] P. Bonche and D. Vautherin, *Nucl. Phys.* **A372**, 496 (1981).